RSC Advances

PAPER

View Article Online
View Journal | View Issue

Cite this: *RSC Adv.*, 2022, **12**, 33180

A fluorescent molecular rotor for the *in situ* imaging of latent fingerprints†

Na-Eun Choi, Eun-Ji Kim and Jiyoun Lee *

Received 24th October 2022
Accepted 14th November 2022

DOI: 10.1039/d2ra06728e

rsc.li/rsc-advances

Efficient techniques for developing latent fingerprints are invaluable resources to solve crimes. In this work, we developed a fluorescent molecular rotor probe that responds to hydrophobic and viscous environments and visualizes latent fingerprints with level 3 details. We believe that the simple and convenient features of **LFP-1** will benefit forensic practice.

Introduction

Fingerprints are regarded as a crucial piece of evidence in criminal investigations because they are unique biometric identifiers. While DNA profiling serves as a conclusive method in modern forensics, fingerprints still provide a reliable alternative to identify a person of interest. Commonly used techniques for collecting latent fingerprints are based on the visualization of residual moisture and grease on surfaces *via* application of various materials and chemicals.[1] Black powder (dry method) and ninhydrin solution (wet method) are the two most widely used methods.[1] The dry method is readily accessible at crime scenes, although it requires dusting and taping procedures, which can damage the fingerprint details and any potential evidence nearby. The wet method is applicable for a wide range of surfaces, including paper and cloth; however, it usually requires additional development procedures that are time-consuming or require expensive instruments.

A fingerprint is created by sweat secretions, which comprise 98% water and organic and inorganic substances mixed as an emulsion.[2] The organic components in sweat mostly consist of amino acids and lipids, whereas the inorganic components consist of ions.[3] The initial composition of a fingerprint significantly changes over time. The volatile components are rapidly evaporated, leaving behind only 2% of the original mass within 3 days.[3] The resulting fingerprint becomes viscous and brittle and is highly susceptible to physical erosion.[4] Given that latent fingerprints discovered at crime scenes are aged from a few hours to several years, a reliable method to detect both fresh and aged latent fingerprints would be an invaluable tool for criminal investigations.

Ninhydrin, 1,2-indandione, and 1,8-diazafluoren-9-one (DFO) are routinely used chemicals for collecting latent fingerprints (Fig. 1a). These reagents react with amino acids and generate visible (ninhydrin) or fluorescent signals (1,2-indandione and DFO) on various surfaces. While these are well-established methods acceptable for use in the courtroom, they all require multiple developing agents with heating and drying.[5] Additionally, to detect the fingerprints developed with 1,2-indandione and DFO, specialized lighting equipment with a filter system is needed.[5] To overcome these limitations, fluorescent small molecules and polymeric particles with minimal processing steps have been developed.[6,7] More recently, fluorophores with aggregation-induced emission (AIE) have been reported to offer potential improvement over conventional reagents[8,9] because AIE-based reagents display strong fluorescence enhancement upon adhering to fingerprints ('turn-on' response) and exhibit great sensitivity, allowing the detection of level 2–3 details. As described in Fig. 1b, various AIE luminogens have been developed for fingerprint detection. These reagents have an AIE-active structural core, such as tetraphenylethylene (TPE),[10] fluorene diphenylimidazole (FDIP),[11] DPPS,[12] and triphenylamine (TPA).[9]

On the basis of previous findings, we hypothesized that a lipophilic fluorophore with solvatochromic properties can generate fluorogenic signals upon adhering to lipids in latent fingerprints. In addition, if we incorporate an additional AIE active core, the lipid-generated signals will be further boosted

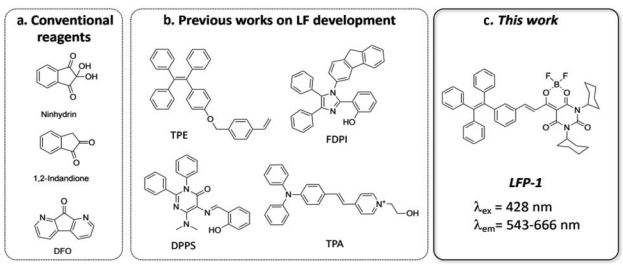

Fig. 1 Structures of the reagents used for latent fingerprinting (a) widely used reagents; (b) recently reported examples; (c) **LFP-1** in this work.

School of Biopharmaceutical and Medical Sciences, Sungshin University, Seoul 01133, Republic of Korea. E-mail: jlee@sungshin.ac.kr

† Electronic supplementary information (ESI) available: Supplementary figures (Fig. S1–S6) and characterization data. See DOI: 10.1039/d2ra06728e.

by AIE, which will enhance specific signals from aged or faint fingerprints with low moisture content. Most previously developed probes have amphiphilic properties and can be expected to bind to both organic and inorganic components and to promote AIE. However, we decided to focus on lipid components that can be preserved for a long time and provide highly fluorogenic signals but can also be developed with minimal processing without using mixed solvent systems. Herein, we introduce a fluorescent probe incorporating a lipid-responsive dioxaborine complex with the TPE core, **LFP-1** (latent fingerprint probe-1), for the detection of latent fingerprints, as shown in Fig. 1c. Klymchenko and coworkers reported ultrabright merocyanine fluorophores containing a barbiturate-based dioxaborine complex,[13] and they demonstrated a significant enhancement in the quantum yield in response to polarity and viscosity. Considering that fingerprints are formed by emulsified lipid secretions that become viscous over time, we consider that the dioxaborine core has optimal properties for lipid-dependent visualization of latent fingerprints. In this report, we synthesized and characterized the spectroscopic properties of **LFP-1**. **LFP-1** demonstrates a shifted emission in response to solvent polarity but also exhibits fluorescence enhancement in a viscous environment, making it suitable for rapid *in situ* imaging of latent fingerprints. We further tested **LFP-1** to detect latent fingerprints on various surfaces. Once sprayed, **LFP-1** can be used to quickly visualize latent fingerprints at high resolution (level 3 details) and clearly develop aged fingerprints. The redshifted emission in polar solvents is particularly useful to distinguish developed fingerprints from the background without any posttreatment, such as heating and washing. Finally, we examined the developed fingerprints using fluorescence microscopy and scanning electron microscopy (SEM), confirming that **LFP-1** specifically binds to lipid deposits in the ridge regions of fingerprints.

Results and discussion

Chemistry

LFP-1 was prepared in three steps by following the previously described procedure,[13] as described in Scheme 1. The dioxaborine fragment (**1**) was synthesized by reacting commercially available dicyclohexylbarbituric acid with acetic anhydride followed by adding $BF_3 \cdot OEt_2$. The AIE-active tetraphenylene core (**2**) was prepared *via* a Suzuki coupling reaction. The desired fluorophore **LFP-1** was synthesized by condensing **1** and **2** in anhydrous dichloroethane in the presence of piperidine as a catalyst. The final compound was characterized by ^1H, ^{13}C, and ^{19}F NMR and ESI-mass spectrometry.

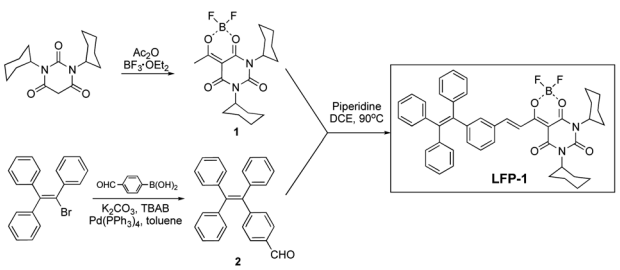

Scheme 1 Synthesis of LFP-1.

Spectroscopic properties

The optical properties of **LFP-1** were examined in various solvents, as shown in Table 1 and Fig. S1 (ESI†). **LFP-1** is observed to absorb light at wavelengths ranging from 423 nm to 438 nm; however, it demonstrates a greatly redshifted emission in response to solvent polarity. Specifically, **LFP-1** shows a maximum emission at 543 nm in heptane, which is the least polar solvent among all those tested (dielectric constant = 1.92). As the solvent polarity is increased, the emission maxima is also increased up to 666 nm (in DMSO, dielectric constant = 46.9). We believe that the significant dipole moment present in **LFP-1** and the push–pull interaction between the tetraphenyl-ethylene group and dioxaborine core contribute to strong solvatochromism. Dioxaborines have enol and ketone oxygens coordinated with boron difluoride, exhibiting good photostability and high quantum yield similar to BODIPY. The Stokes shifts are also large (from 115 nm to 233 nm), which is likely due to the contribution of the AIE-active TPE to the charge transfer process as an energy donor.[14]

To further examine the AIE properties and push–pull emission responses in mixed solvent systems, we tested different sets of mixtures, THF–water, heptane–THF, and heptane–corn oil mixtures. As shown in Fig. 2a and b, when we determined the emission profile of **LFP-1** in a THF–water mixture, we were able to observe the aggregation-induced emission enhancement (AIEE) starting from the mixture containing 40% water to 100% water solution, and the fluorescence signal increased up to 13-fold. **LFP-1** appears to form aggregates that exert bright orange fluorescence with the emission maxima at 608 nm. These soluble aggregates are homogeneously dispersed in solution exhibiting strong AIEE. **LFP-1** also exhibited AIEE phenomenon in the solid state, as shown in Fig. 2c, the solid looks bright red under daylight but also demonstrates strong orange fluorescence under 405 nm light illumination. Next, we measured the

Table 1 Spectroscopic properties of LFP-1 in various solvents

Solvent	λ_{abs} (nm)	ε^a (M^{-1} cm^{-1})	λ_{em} (nm)	ϕ^b	κ^c
Heptane	428	37 166	543	0.07	1.92
Toluene	444	38 526	587	0.03	2.38
1,4-Dioxane	438	40 900	604	0.05	2.21
Tetrahydrofuran	436	48 788	626	0.02	7.52
Dichloromethane	443	45 907	648	0.02	9.08
Isopropanol	438	59 386	627	0.02	18.3
EtOH	435	44 291	643	0.02	24.6
MeOH	423	48 901	631	0.003	32.6
Acetone	427	54 595	655	0.006	21.0
DMSO	433	56 427	666	<0.001	46.7
Water	450	16 683	608	0.09	78.5

[a] ε: molar extinction coefficient. [b] ϕ: quantum yield. [c] κ: solvent dielectric constant taken from https://organicchemistrydata.org/solvents/

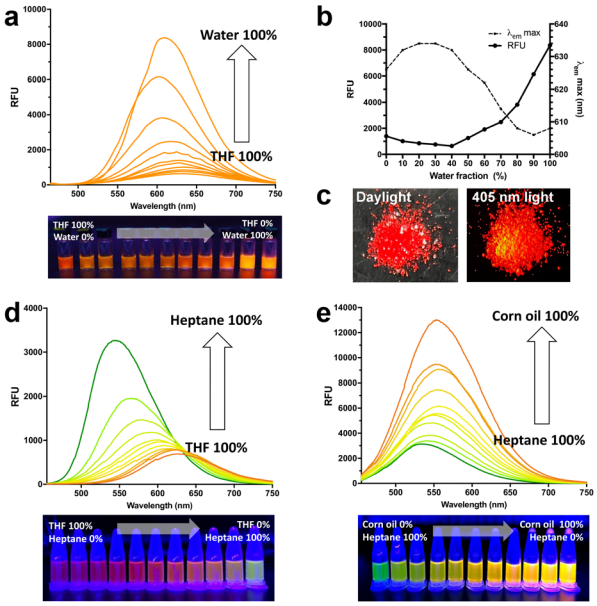

Fig. 2 (a) Emission spectra of **LFP-1** in water–THF mixtures; (b) changes in relative fluorescence signals and emission maxima in different fractions of water–THF mixtures; (c) real color photographs of **LFP-1** solids under daylight and 405 nm light; (d) emission spectra for **LFP-1** in THF–heptane mixtures and (e) emission spectra for **LFP-1** in heptane–corn oil mixtures (λ_{ex} = 428 nm).

emission profile of **LFP-1** in a heptane-THF mixture (Fig. 2d and S2a†). The emission maxima gradually shifted from 624 nm to 543 nm, and the signal intensity increased up to 4-fold as the heptane fraction is increased from 10% to 100%. The emission wavelength is redshifted as the more polar THF fraction is increased but also appears to show reduced overall fluorescence compared to the 100% heptane solution. Given that previously developed dioxaborine dyes demonstrate a viscosity-sensitive fluorescence response,[15] we decided to examine the push–pull emission of **LFP-1** in viscous environments, such as heptane-corn oil mixtures. As shown in Fig. 2e, **LFP-1** demonstrates a 4-fold enhancement in the fluorescence signals in response to increasing viscosity of up to 100% corn oil exhibiting bright yellow fluorescence. Interestingly, the emission maxima are slightly shifted, but to a much lesser extent (534 nm to 556 nm, Fig. S2b†) than the heptane–THF mixtures. This enhanced emission implies that the increased viscosity restricts the intramolecular rotation of **LFP-1**, thus facilitating additional twisted intramolecular charge transfer (TICT), which corresponds to the observations reported previously for dioxaborine derivatives.[13,16] In a non-polar, viscous environment, the TPE core appears to act as an electron donor rather than AIEgen, making **LFP-1** an efficient molecular rotor that can respond to solvent polarity and viscosity. As summarized in Fig. 3, **LFP-1** responds to the changes in polarity and viscosity while acting as a fluorescent molecular rotor but also exhibits AIEE in highly polar solvents such as THF–water mixture. We think these characteristics are suitable for imaging latent fingerprints, consisting of emulsified sweat secretions confined along the fingermarks.

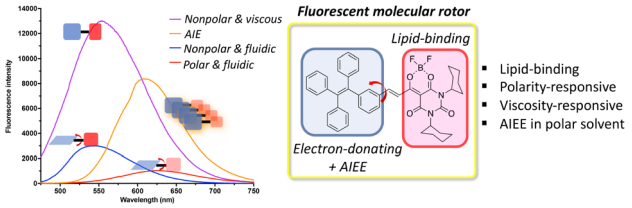

Fig. 3 Comparison of relative fluorescence intensities in different environment and structural characteristics of **LFP-1**.

Detection of latent fingerprints

We next used **LFP-1** to develop latent fingerprints. To determine the optimal development conditions, we considered the following factors: first, the solvent system needs to be readily applicable and favorable for long-term storage; second, the spraying solution must be minimally toxic; and third, the overall development process should be simple and brief without any additional heat, chemical treatment, or extensive washing and drying procedures. Therefore, we excluded the use of volatile organic solvents such as toluene and THF. We selected ethanol and water as our testing solvents for the development. Before proceeding, we determined the cytotoxicity of **LFP-1** by MTT assays, and **LFP-1** was found to exhibit no toxicity up to 50 μM (Fig. S3, ESI†). Latent fingerprints were prepared by rubbing the finger with the forehead and depositing fingerprints onto glass slides, which were then briefly sprayed with a solution of **LFP-1** and dried in air. The resulting glass slides were photographed using a digital camera under a 405 nm light LED lamp. When we used an aqueous solution of **LFP-1**, the solution seemed to bind more readily to the surface of the glass rather than the deposited fingerprints, as demonstrated in Fig. S4 (ESI†). Because the glass surface has polar residues, it showed bright red fluorescence under 405 nm light illumination. In contrast, the fingerprints were vaguely visible or exhibited pale yellow color. Therefore, we think that aqueous solution is not suitable for optimal interaction with fingerprints. On the other hand, as shown in Fig. 4a, fingerprints are clearly visible upon spraying the solution of **LFP-1** in ethanol, and their signal intensities increase with increasing dye concentration. More importantly, each fingerprint exhibits bright yellow fluorescent signals, whereas the rest of the glass slide shows a dark pink color, distinguishing the fingerprints from the background without additional postprocessing. While fingerprints are visible at all four concentrations, we decided to use **LFP-1** at 25 μM to develop latent fingerprints with visual clarity.

Next, we wanted to develop aged fingerprints with **LFP-1**. In many cases, fingerprints found in crime scenes and evidentiary materials can be several days to years old, making the fingerprints dry and brittle. Developing old fingerprints poses a challenging task because currently available methods, such as powder dusting or superglue fuming, are severely affected by the moisture content of fingerprints but can also potentially damage the evidence. We believe that because old fingerprints are more viscous than freshly deposited fingerprints, **LFP-1** can provide a suitable method to visualize aged fingerprints without

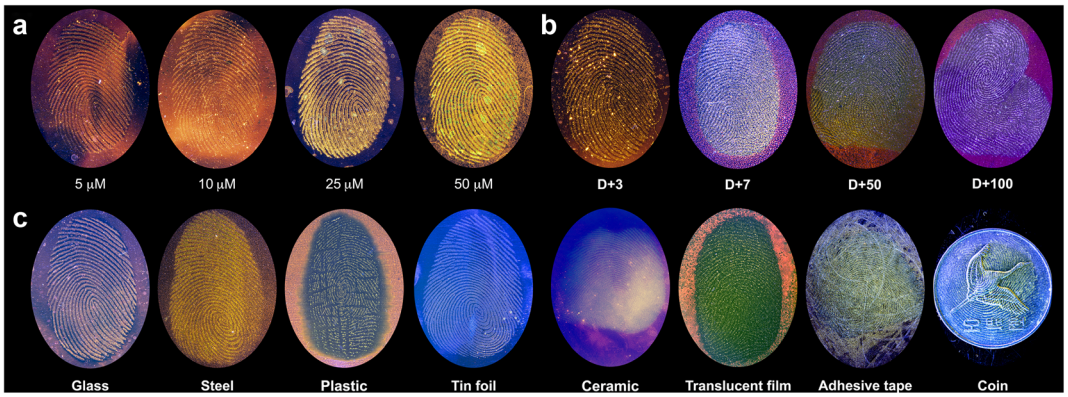

Fig. 4 (a) Photographs of fingerprints deposited on glass slides developed with **LFP-1** at different concentrations. (b) Photographs of aged fingerprints developed with **LFP-1**. (c) Photographs of fingerprints developed with **LFP-1** on various surfaces.

damage. To test our hypothesis, we prepared glass slides with fingerprints that were left open to air for a defined period (3 days to 100 days) and then sprayed with **LFP-1** (Fig. 4b) for visualization. All fingerprints were not only found to be clearly visible regardless of their age, but older fingerprints exhibited more intense fluorescence in accordance with our initial hypothesis.

Because TPE molecules are also known to visualize fingerprints *via* AIE mechanism,[17] we tested compound **2**, the TPE fragment in **LFP-1**, for additional spectroscopic analysis and latent fingerprint visualization. As described in Fig. S5 (ESI†), compound **2** showed relatively weak fluorescence and did not appear to demonstrate polarity- or viscosity-dependent emission enhancement that was observed with **LFP-1**; when it was tested in heptane/corn oil mixture, the fluorescence signals only increased when the fraction of heptane increased, contrasting to the observations with **LFP-1**. Furthermore, when we sprayed an ethanol solution of **2** over latent fingerprints, we were unable to observe clear fluorescence signals, suggesting that the TPE core itself is not enough for AIE-dependent visualization of fingerprints. We think that **LFP-1** visualizes latent fingerprints mainly by acting as a molecular rotor. AIEE-derived from the TPE core may help boost signals in the freshly deposited fingerprints, which have more moisture content than aged fingerprints.

To further test the practicality of our probe, we also visualized latent fingerprints on various substances. As demonstrated in Fig. 4c, **LFP-1** can be used to successfully develop latent fingerprints on non-porous surfaces such as glass, steel, plastic, and tinfoil with high resolution. Due to the reflection of light from the surface, the photographed images of some objects such as tin foil, ceramic, and coin have a blueish tint. We also tested some objects with uneven or curved surfaces, including a ceramic dish, translucent film, adhesive tape, and a coin, and we were able to identify clearly visible fingerprints. It should be noted that we were unable to process the fingerprints from porous surfaces such as wood, paper, and leather, likely because these substances absorbed the sprayed solution, which quickly dispersed through their porous structure. Because most evidentiary materials have curved surfaces, we also wanted to see if the developed fingerprints can be transferred to fingerprinting tape for further analysis by using a fluorescence scanner in the green channel (excitation at 520–545 nm, emission at 577–613 nm) (Fig. S6, ESI†). The fluorescence signals in the scanned images correspond to the images taken with a digital camera, providing bright and high-quality images of the latent fingerprints. Thus, the fingerprint developed using **LFP-1** can be additionally collected by the taping method, which is useful for identifying fingerprints from curved or uneven surfaces.

Fingerprints from individuals are known to contain three levels of information.[6] The first level, or level 1, includes ridge patterns such as arch, loop and whorl, which are mainly used for exclusion and not identification. The second level details include more specific features, such as a lake, ridge ending, and bifurcation, and can be used to distinguish unique fingerprints. The third level details cover microscopic features, including edge contours, sweat pore distribution, ridge path deviation, and specific scars, which provide robust and definitive details for individual identification. To examine these details in the developed fingerprints, we analyzed the photograph of the fingerprint on a glass surface, as shown in Fig. 5. Level 1 and 2 details, such as core, ridge endings, island, and bifurcation, are clearly visible in Fig. 5. The color intensity across the red bar in Fig. 5a was measured and plotted using gray values, demonstrating a high contrast between the fingerprint ridges and furrows, as well as sweat pores. When this image is magnified (Fig. 5b), level 2 and 3 details, including sweat pore distribution, edge contour, and line shape, can be determined clearly by visual inspection. Overall, **LFP-1** can provide all three levels of detailed information for individual fingerprints.

FE-SEM and fluorescence microscopic image analysis

To further investigate the development mechanism for **LFP-1**, we examined the surface morphology of the developed fingerprints by using field emission scanning electron microscopy (FE-SEM) and fluorescence microscopy. The FE-SEM images shown in Fig. 6a demonstrate that **LFP-1** is evenly distributed on the fingerprint ridges, and not on the furrows. Upon examining the specific region of the fingerprint in more detail, as shown in panels 2 and 3 of Fig. 6a, we observe small aggregates dispersed

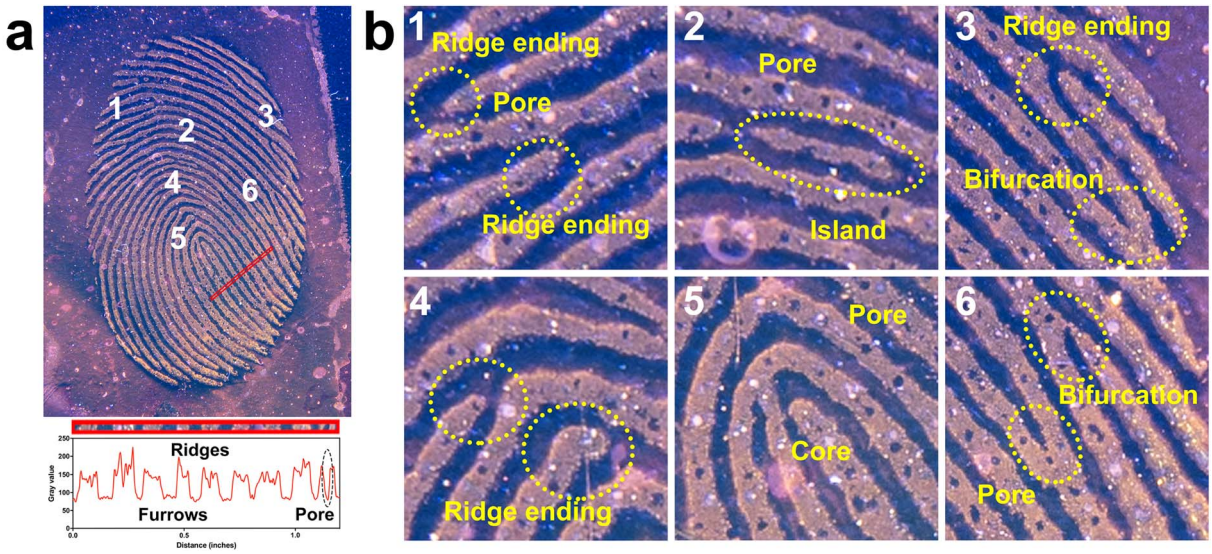

Fig. 5 (a) Photograph of a fingerprint developed with **LFP-1** on glass surface and a gray value analysis for the area of the photograph indicated by the red bar. (b) Magnified regions indicated by the numbers in (a).

across the ridge area. We think that once sprayed, **LFP-1** is concentrated in the lipid components of the fingerprint residues, which leads to the emission of intense fluorescence.

Next, to investigate how **LFP-1** adheres to fingerprints, we acquired fluorescence images of the developed fingerprints with a fluorescence microscope. Fingerprints were deposited onto glass slides and left in the air for a defined period (from 15 days to 60 days), and then **LFP-1** was sprayed before fluorescence imaging. As shown in Fig. 6b, on day 1, we observed a similar distribution pattern for **LFP-1** as observed in the SEM images. Interestingly, over time, residues in fingerprints become dense with granular patterns, but an increasing number of large aggregates also appear, suggesting that once moisture evaporates, the remaining components, such as fatty acids and proteins, are reconstructed into granular structures with aggregates. Upon analysis of the fluorescence images, we found that these large aggregates correspond to bright fluorescence signals, suggesting that they are mainly composed of lipids. Taken together, these results indicate that **LFP-1** selectively interacts with the lipid components of fingerprints and provides a reliable and convenient method to visualize latent fingerprints that are both fresh and old.

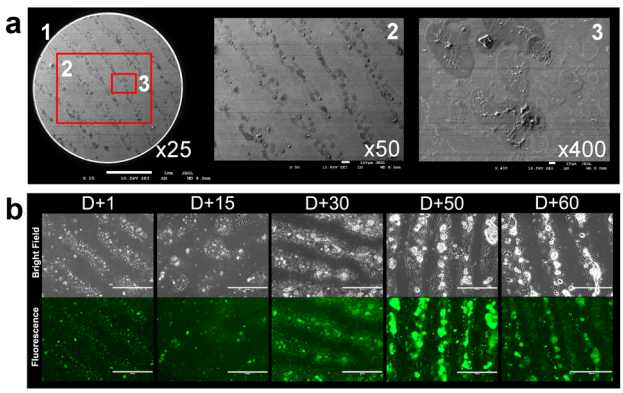

Fig. 6 (a) FE-SEM images of the fingerprint developed with **LFP-1** (SEM at a magnification of ×25 (1), ×50 (2), and ×400 (3)); (b) brightfield images (top) and fluorescence images (bottom) of the fingerprint at the given time period developed with **LFP-1** (scale bars: 400 μm).

Conclusion

In this study, we developed a fluorescent molecular rotor, **LFP-1**, for facile *in situ* visualization of latent fingerprints. **LFP-1** was synthesized in three steps with a good overall yield and demonstrated a polarity-responsive emission shift as well as AIEE characteristics. In addition, this probe has a molecular rotor property that induces fluorescence enhancement in a nonpolar viscous environment. The optical properties of **LFP-1** are particularly suitable for the detection of latent fingerprints because it provides a selective turn-on response upon adhering to lipid components of fingerprints, and these effects are even enhanced in aged fingerprints. **LFP-1** can be applied on various surfaces, including glass, aluminum foil, coin, and ceramics, and the developed fingerprints can be further processed by the taping method. The developed fingerprints clearly show all three levels of details (ridge patterns, shapes, bifurcation and sweat pore distributions); thus, **LFP-1** provides reliable and definitive information for personal identification. Because fingerprint processing is routinely performed in crime labs, the safety, toxicity and simplicity of the development procedures are also important. **LFP-1** is not cytotoxic up to 50 μM and can be dissolved in ethanol and sprayed, and blue light illumination gives clearly developed fingerprints with level 3 details. The turn-on fluorescence response of **LFP-1** is also beneficial for convenient processing and preserving evidence because it does not require any posttreatment, such as washing and fuming. We believe that **LFP-1** can provide a simple, practical, and highly efficient method for the detection of latent fingerprints and is

anticipated to be used in crime scenes and forensic laboratories in the near future.

Experimental

Chemistry

General methods. Unless otherwise noted, materials and solvents were purchased from commercial suppliers and used without further purification. Flash chromatography was carried out using silica gel 60 (Merck-Millipore). NMR spectra were obtained using a Varian JNM-ECZ500R/S1 spectrometer (JEOL). NMR chemical shifts are reported in ppm and referenced to the residual protonated solvent. Mass spectral analyses were carried out using an Agilent 6130 single quadrupole liquid chromatography and mass spectrometer system.

Synthesis

*Synthesis of 6,8-dicyclohexyl-2,2-difluoro-4-methyl-2,8-dihydro-5H-1l3,2l4-[1,3,2]dioxa-borinino[6,5-d]pyrimidine-5,7(6H)-dione (compound **1**).* Compound **1** was synthesized by following the previously published procedure.[13] Acetic anhydride (360 μl) was added to 1,3-dicyclohexylbarbituric acid (657.9 mg, 2.25 mmol), and the mixture was heated to 95 °C. $BF_3 \cdot OEt_2$ (383.23 mg, 2.70 mmol, 1.2 eq.) was added to the hot reaction mixture, following which the solution became homogeneous and yellowish. After 30 minutes, TLC was used to show that the reaction was complete. The solvent was evaporated, and MeOH was added to filter off the white solid to give 661.6 mg of **1** as a white powder (yield = 67.7%). ESI-MS: *m*/*z* calcd for $C_{18}H_{25}BF_2N_2O_4$ $[M + H]^+$: 383.19; found: 383.1. ^{1}H-NMR (500 MHz, $CDCl_3$) δ 4.76 (m, 2H), 2.93–2.66 (m, 3H), 2.33–2.21 (m, 4H), 1.86 (t, J = 14.6 Hz, 4H), 1.75–1.60 (m, 6H), 1.41–1.16 (m, 6H).

*Synthesis of 4-(1,2,2-triphenylethyl)benzaldehyde (compound **2**).* Compound **2** was synthesized by following the previously published procedure.[18] 2-Bromo-1,1,2-triphenylethylene (952.9 mg, 2.84 mmol) and 4-formylphenylboronic acid (639.3 mg, 4.26 mmol, 1.5 eq.) were dissolved in toluene (15 ml), and then tetrabutylammonium bromide (92.0 mg, 0.29 mmol, 0.1 eq.) in 2 M K_2CO_3 aqueous solution (4 ml) was added to the reaction flask. The reaction mixture was stirred for 30 min at room temperature, $Pd(PPh_3)_4$ (5 mg) was added and refluxed for 24 h at 90 °C. The progress of the reaction was monitored by TLC using hexane : DCM (2 : 1). After completion of the reaction, the mixture was cooled to room temperature and poured into water. The product was extracted with ethyl acetate and dried over anhydrous $MgSO_4$, and the solvent was evaporated. The crude product was subjected to silica gel column chromatography for purification. Yield = 696.2 mg (50.5%). ESI-MS: *m*/*z* calcd for $C_{27}H_{20}O$ $[M + H]^+$: 361.15; found: 361.1. ^{1}H NMR (500 MHz, $CDCl_3$) δ 9.89 (s, 1H), 7.60 (d, J = 8.6 Hz, 2H), 7.18 (d, J = 8.0 Hz, 2H), 7.10–7.12 (m, 9H), 7.02–6.99 (m, 6H).

*Synthesis of **LFP-1**.* **LFP-1** was synthesized by following the previously published procedure[13] with minor modifications. Compound **1** (25.3 mg, 0.066 mmol, 2 eq.) and compound **2** (11.6 mg, 0.032 mmol, 1 eq.) in 1,2-dichloroethane (1 ml) were placed into a two-neck round bottom flask, and then piperidine (5 μl) was added to the flask. The reaction mixture was stirred for 1.5 h under refluxing, and the completion of the reaction was confirmed by LC/MS. After that, the solvent was evaporated under reduced pressure, and the residue was separated by column chromatography using hexane : toluene (1 : 3). Orange red solid. Yield = 20.1 mg (84.1%). ESI-MS: *m*/*z* calcd for $C_{45}H_{43}BF_2N_2O_4$ $[M + H]^+$: 725.33; found: 725.3. ^{1}H NMR (500 MHz, $CDCl_3$) δ 8.42 (d, J = 15.3 Hz, 1H), 8.18 (d, J = 15.6 Hz, 1H), 7.46 (d, J = 8.4 Hz, 2H), 7.17–7.08 (m, 12H), 7.05–7.00 (m, 4H), 4.86–4.74 (m, 2H), 2.37–2.27 (m, 7H), 1.86 (m, 4H), 1.76 (m, 2H), 1.67–1.62 (m, 4H), 1.41–1.18 (m, 6H). ^{13}C NMR (126 MHz, $CDCl_3$) δ 181.9, 167.3, 159.6, 151.9, 149.1, 148.4, 143.3, 143.2, 143.1, 143.1, 140.0, 138.0, 132.3, 131.5, 131.4, 131.4, 129.7, 129.1, 128.3, 128.0, 128.0, 127.8, 127.2, 126.9, 125.4, 119.2, 93.4, 58.0, 55.4, 29.8, 29.4, 28.8, 26.4, 26.3, 25.3, 25.0, 21.5. ^{19}F-NMR (471 MHz, $CDCl_3$) δ −143.92.

Spectroscopic measurements

UV-Vis absorbance and fluorescence measurements were performed using a Spectramax M5 multimode microplate reader (Molecular Devices). A 50 mM stock solution of **LFP-1** in DMSO was dissolved in 1 mL of each solvent to a final concentration of 25 μM. Absorbance and fluorescence spectra were obtained by using quartz cuvettes (Hellma GmbH) at room temperature. Fluorescence quantum yields were determined according to the following equation: $\Phi_{f,x} = \Phi_{f,st} \times (F_x/F_{st}) \times (f_{st}/f_x) \times (n_x/n_{st})$,[18] where Φ_f, F, f, n denote the fluorescence quantum yield, absorbance at the excitation wavelength, area under the emission peak, and refractive index of the solvent, respectively. The subscripts x and st denote the sample and standard, respectively. $\Phi_{f,st}$ for fluorescein in isopropanol (Φ = 0.92)[19] was used as a reference.

Cell viability assay

HeLa cells were grown in Dulbecco's modified Eagle's medium (DMEM, GIBCO) supplemented with 10% (vol/vol) FBS and antibiotics (100 mg per ml penicillin/streptomycin mix) in a humidified atmosphere at 37 °C with 5% CO_2. Cell viability was assessed using a thiazolyl blue tetrazolium bromide (MTT, Sigma-Aldrich) assay. A total of 3×10^4 cells were plated onto 96-well plates (BD Falcon). After 1 day, the cells were treated with DMSO or **LFP-1** for 2 h. Then, MTT solution (final concentration, 1 mg mL^{-1}) was added to each well, and the plates were incubated for an additional 2 h at 37 °C. Formazan crystals were solubilized by adding DMSO, and the absorbance was measured at a wavelength of 550 nm. OD values from each well were subtracted from the DMSO control, and the percent cell viability was calculated.

Development of latent fingerprints using LFP-1

The latent fingerprints were developed on various subjects. The volunteers (females, ages 24 to 26) washed their hands with soap first and then gently rubbed their fingers across the forehead. The fingers were pressed on different surfaces at room temperature. The **LFP-1** solution (25 μM, ethanol) was sprayed onto the latent fingerprints and then dried in air. The developed fingerprint images were photographed by using a Leica Q2 digital camera under 405 nm LED light irradiation. Fluorescence images of the fingerprints transferred to forensic tape

were scanned by a ChemiDoc MP imaging system (Bio-Rad) using the green channel settings (excitation at 520–545 nm, emission at 577–613 nm).

FE-SEM and fluorescence imaging

High-resolution fingerprint images were recorded by using a JSM-7500F (JEOL) field emission scanning electron microscope. Fluorescence microscopic images were captured by an EVOS FL imaging system (Thermo-Fisher Scientific) with a 20× objective in the green channel.

Conflicts of interest

There are no conflicts to declare.

Acknowledgements

This work was supported by the Sungshin Women's University Research Grant of H20210042.

Notes and references

1 H. M. Daluz, *Fundamentals of Fingerprint Analysis*, CRC Press, London, UK, 2018.
2 S. Cadd, M. Islam, P. Manson and S. Bleay, *Sci. Justice*, 2015, **55**, 219–238.
3 A. Girod, R. Ramotowski and C. Weyermann, *Forensic Sci. Int.*, 2012, **223**, 10–24.
4 S. P. Wargacki, L. A. Lewis and M. D. Dadmun, *J. Forensic Sci.*, 2008, **53**, 1138–1144.
5 M. Levin-Elad, Y. Liptz, K. L. Bar-Or and J. Almog, *Forensic Sci. Int.*, 2017, **271**, 8–12.
6 J. Lian, F. Meng, W. Wang and Z. Zhang, *Front. Chem.*, 2020, **8**, 594864.
7 (*a*) E. Prabakaran and K. Pillay, *J. Mater. Res. Technol.*, 2021, **12**, 1856–1885; (*b*) H. Chu, L. Yang, L. Yu, J. Kim, J. Zhou, M. Li and J. S. Kim, *Coord. Chem. Rev.*, 2021, **449**, 214208; (*c*) P. Zhang, M. Xue, Z. Lin, H. Yang, C. Zhang, J. Cui and J. Chen, *Sens. Actuators, B*, 2022, 132049; (*d*) R. Zou, Y. Yu, H. Pan, P. Zhang, F. Cheng, C. Zhang, S. Chen, J. Chen and R. Zeng, *ACS Appl. Mater. Interfaces*, 2022, **14**, 16746–16754.
8 (*a*) R. Suresh, S. K. Thiyagarajan and P. Ramamurthy, *Sens. Actuators, B*, 2018, **258**, 184–192; (*b*) M. K. Ravindra, K. M. Mahadevan, R. B. Basavaraj, G. P. Darshan, S. C. Sharma, M. S. Raju, G. R. Vijayakumar, K. B. Manjappa, D. Y. Yang and H. Nagabhushana, *Mater. Sci. Eng., C*, 2019, **101**, 564–574; (*c*) N. Kumar, Udayabhanu, K. M. Mahadevan and G. Nagaraju, *J. Sci.: Adv. Mater. Devices*, 2020, **5**, 520–526; (*d*) H.-Y. Wang, C.-Y. Tan, K.-K. Yu, K. Li, Y.-H. Liu and X.-Q. Yu, *Mater. Chem. Front.*, 2021, **5**, 6603–6610; (*e*) M. K. Ravindra, G. P. Darshan, D. R. Lavanya, K. M. Mahadevan, H. B. Premkumar, S. C. Sharma, H. Adarsha and H. Nagabhushana, *Sci. Rep.*, 2021, **11**, 16748; (*f*) N. Kumar, Udayabhanu, A. Ali Alghamdi, R. B. Basavaraj, K. M. Mahadevan and G. Nagaraju, *Luminescence*, 2021, **36**, 1013–1023; (*g*) M. Ahmad, G. Kumar, V. Luxami, S. Kaur, P. Singh and S. Kumar, *New J. Chem.*, 2021, **45**, 7705–7713.
9 Y. L. Wang, C. Li, H. Q. Qu, C. Fan, P. J. Zhao, R. Tian and M. Q. Zhu, *J. Am. Chem. Soc.*, 2020, **142**, 7497–7505.
10 A. H. Malik, A. Kalita and P. K. Iyer, *ACS Appl. Mater. Interfaces*, 2017, **9**, 37501–37508.
11 Y. Wang, H. Liu, Z. Chen and S. Pu, *Spectrochim. Acta, Part A*, 2021, **245**, 118928.
12 P. Singh, H. Singh, R. Sharma, G. Bhargava and S. Kumar, *J. Mater. Chem. C*, 2016, **4**, 11180–11189.
13 M. Collot, T. K. Fam, P. Ashokkumar, O. Faklaris, T. Galli, L. Danglot and A. S. Klymchenko, *J. Am. Chem. Soc.*, 2018, **140**, 5401–5411.
14 N. Balsukuri, N. Manav, M. Y. Lone, S. Mori, A. Das, P. Sen and I. Gupta, *Dyes Pigm.*, 2020, **176**, 108249.
15 A. S. Klymchenko, *Acc. Chem. Res.*, 2017, **50**, 366–375.
16 (*a*) I. A. Karpenko, Y. Niko, V. P. Yakubovskyi, A. O. Gerasov, D. Bonnet, Y. P. Kovtun and A. S. Klymchenko, *J. Mater. Chem. C*, 2016, **4**, 3002–3009; (*b*) L. A. Padilha, S. Webster, O. V. Przhonska, H. Hu, D. Peceli, T. R. Ensley, M. V. Bondar, A. O. Gerasov, Y. P. Kovtun, M. P. Shandura, A. D. Kachkovski, D. J. Hagan and E. W. Van Stryland, *J. Phys. Chem. A*, 2010, **114**, 6493–6501; (*c*) Z. R. Grabowski, K. Rotkiewicz and W. Rettig, *Chem. Rev.*, 2003, **103**, 3899–4032.
17 (*a*) X. Jin, R. Xin, S. Wang, W. Yin, T. Xu, Y. Jiang, X. Ji, L. Chen and J. Liu, *Sens. Actuators, B*, 2017, **244**, 777–784; (*b*) Y. Li, L. Xu and B. Su, *Chem. Commun.*, 2012, **48**, 4109–4111.
18 X. Zhang, Z. Chi, B. Xu, C. Chen, X. Zhou, Y. Zhang, S. Liu and J. Xu, *J. Mater. Chem.*, 2012, **22**, 18505–18513.
19 D. Magde, R. Wong and P. G. Seybold, *Photochem. Photobiol.*, 2002, **75**, 327–334.